M of the total plate separation (Fig. 3B). The remaining fraction ($1 - M$) is accommodated by slip on normal faults that initiate near the axis and are subsequently pushed off-axis by magmatic intrusion at a rate that increases with M (*24*, *25*). As a fault encounters progressively thicker off-axis lithosphere, the work required to keep it active increases until it becomes mechanically favorable to abandon it in favor of a new fault forming closer to the axis (Fig. 3B). Mechanical scaling laws (*12*) predict that thick or rapidly thickening lithosphere with a robust magma supply (high M) produces relatively short-lived, and therefore closely spaced, faults (*24*, *25*). Upon parameterizing axial lithospheric thickness, thickening rate, and M, versus spreading rate through empirical fits to observations (Fig. 3A, inset, and fig. S2), we use these mechanical scaling laws to predict a decrease in abyssal hill spacing from ~10 to ~2.5 km with increasing spreading rate, following the trend of the observations (Fig. 3A). Thus, the systematic variations in abyssal hill fabric with spreading rate are best explained by a model of tectono-magmatic extension under a steady magma input.

Steady magma input is an oversimplification of the ridge magmatic system, even without climatic variations in magma flux (*26*, *27*). Thus, we consider the possibility that an oscillating magma input could alter the above behavior by directly affecting the duration that individual faults remain active (*28*), and therefore imprint the seafloor fabric. We performed two-dimensional numerical simulations of normal fault growth coupled with magmatic injection in the lithosphere that fluctuates on a period τ (*12*). During 85% of the cycle, magma injection accommodates 100% of plate separation (U = 3 cm/year), whereas during the remaining 15%, extension is fully accommodated on faults that form spontaneously in the lithosphere. This scenario maximizes the effects of magmatic modulation but has a time-averaged M equal to 0.85 (*28*).

We ran 12 simulations with τ ranging from 10 to 500 ky. The modeled seafloor shows abyssal hill-like topography, from which we measure the mean fault spacing (Fig. 4A). The spectrum of topography clearly shows that fault spacing expresses a dominant wavelength (Fig. 4B). It also reveals a number of peaks at higher wave numbers (within the Milankovitch range) that cannot be directly interpreted in terms of seafloor length scales. Simulations with short τ consistently produce abyssal hills with a characteristic spacing of ~2 to 4 km, as predicted by the mechanical scaling laws that assume a steady magma input (horizontal red line in Fig. 4C). Simulations with a longer τ, however, reveal a direct control of the forcing period on fault spacing (blue curve). The transition between the two regimes occurs at a period set by the mechanically controlled fault spacing divided by the spreading half-rate, which at intermediate-spreading ridges is ~100 ky. We therefore expect the tectonic fabric of the AAR to be insensitive to even extreme fluctuations in melt supply on Milankovitch frequencies. The spectral peaks observed there (*6*) likely reflect only the mechanically controlled spacing of fault-bounded abyssal hills as shaped by the time-averaged melt supply (M ~ 0.85) (Figs. 3A and 4B).

Each of the three mechanisms of topography development acts as a low-pass filter of melt supply with strong damping of periods shorter than ~100 ky. Therefore, the fingerprints of a climate modulation in MOR melt supply may be found more easily through multichannel seismic imaging of the crust-mantle boundary than through bathymetric analysis. If short-wavelength topography on the base of the crust is observed, comparing its spectral characteristics in crust younger and older than the onset of pronounced glacial cycles would provide a valuable test of the predictions made here and by earlier studies (*6*–*8*).

REFERENCES AND NOTES

1. H. Menard, J. Mammerickx, *Earth Planet. Sci. Lett.* **2**, 465–472 (1967).
2. K. C. Macdonald, P. J. Fox, R. T. Alexander, R. Pockalny, P. Gente, *Nature* **380**, 125–129 (1996).
3. J. A. Goff, Y. Ma, A. Shah, J. R. Cochran, J.-C. Sempéré, *J. Geophys. Res.* **102**, 15521–15534 (1997).
4. D. K. Rea, *Geology* **3**, 77–80 (1975).
5. E. S. Kappel, W. B. F. Ryan, *J. Geophys. Res.* **91**, 13925–13940 (1986).
6. J. W. Crowley, R. F. Katz, P. Huybers, C. H. Langmuir, S. H. Park, *Science* **347**, 1237–1240 (2015).
7. D. C. Lund, P. D. Asimow, *Geochem. Geophys. Geosyst.* **12**, 12009 (2011).
8. M. Tolstoy, *Geophys. Res. Lett.* **42**, 1346–1351 (2015).
9. M. Nakada, H. Yokose, *Tectonophysics* **212**, 321–329 (1992).
10. M. Jull, D. McKenzie, *J. Geophys. Res.* **101**, 21815–21828(1996).
11. P. J. Huybers, C. H. Langmuir, *Earth Planet. Sci. Lett.* **286**, 479–491 (2009).
12. Materials and methods are available as supplementary materials on *Science* Online.
13. A. B. Watts, *Isostasy and Flexure of the Lithosphere* (Cambridge Univ. Press, Cambridge, 2001).
14. J. P. Morgan, Y. J. Chen, *J. Geophys. Res.* **98**, 6283–6297 (1993).
15. J. R. Cochran, *J. Geophys. Res.* **84**, 4713 (1979).
16. B.-Y. Kuo, D. W. Forsyth, E. M. Parmentier, *Geophys. Res. Lett.* **13**, 681–684 (1986).
17. J. M. Sinton, R. S. Detrick, *J. Geophys. Res.* **97**, 197–216 (1992).
18. M. R. Perfit, W. W. J. Chadwick, in *Faulting and Magmatism at Mid-Ocean Ridges*, W. R. Buck *et al.*, Eds. (AGU, Washington DC, 1998), pp. 59–115.
19. R. A. Dunn, D. R. Toomey, *Nature* **388**, 259–262 (1997).
20. W. R. Buck, S. M. Carbotte, C. Z Mutter, *Geology* **25**, 935–938 (1997).
21. S. M. Carbotte, K. C. Macdonald, *J. Geophys. Res.* **99**, 13609–13633 (1994).
22. J. Escartín *et al.*, *Geochem. Geophys. Geosyst.* **8**, Q06005 (2007).
23. J. A. Goff, T. H. Jordan, *J. Geophys. Res.* **93**, 13589–13608 (1988).
24. W. R. Buck, L. L. Lavier, A. N. B. Poliakov, *Nature* **434**, 719–723 (2005).
25. M. D. Behn, G. Ito, *Geochem. Geophys. Geosyst.* **9**, Q08010 (2008).
26. J. P. Canales, J. A. Collins, J. Escartín, R. S. Detrick, *J. Geophys. Res.* **105**, 28411–28425 (2000).
27. E. Bonatti *et al.*, *Nature* **423**, 499–505 (2003).
28. G. Ito, M. D. Behn, *Geochem. Geophys. Geosyst.* **9**, Q09012 (2008).
29. J. Karsten *et al.*, *Intern. Ridge-Crest Res.* **8**, 15–21 (1999).
30. A. Malinverno, R. A. Pockalny, *Earth Planet. Sci. Lett.* **99**, 154–169 (1990).
31. P. A. Cowie, A. Malinverno, W. B. F. Ryan, M. H. Edwards, *J. Geophys. Res.* **99**, 15205–15218 (1994).
32. A. Macario *et al.*, *J. Geophys. Res.* **99**, 17921–17934 (1994).
33. J. Escartín *et al.*, *J. Geophys. Res.* **104**, 10421–10437 (1999).

ACKNOWLEDGMENTS

This work greatly benefited from discussions with P. Canales, A. Soule, S. Carbotte, R. Katz, P. Huybers, and B. Ryan, as well as the constructive feedback from three anonymous reviewers. Funding was provided by NSF grants OCE-1154238 (J.-A.O. and M.D.B), OCE-1155098 (G.I. and S.H.), EAR-1009839 (W.R.B), CNRS support to J.E., a Woods Hole Oceanographic Institution IR&D award to M.D.B, and a Lamont-Doherty Earth Observatory Postdoctoral Fellowship for J.-A.O. The data and model results presented here are included or fully referenced in the supplementary materials.

SUPPLEMENTARY MATERIALS

www.sciencemag.org/content/350/6258/310/suppl/DC1
Materials and Methods
Figs. S1 and S2
References (*34*–*44*)

22 July 2015; accepted 3 September 2015
10.1126/science.aad0715

BIOMATERIALS

A skin-inspired organic digital mechanoreceptor

Benjamin C.-K. Tee,[1]* Alex Chortos,[2]* Andre Berndt,[3]* Amanda Kim Nguyen,[1] Ariane Tom,[3] Allister McGuire,[4] Ziliang Carter Lin,[4] Kevin Tien,[1] Won-Gyu Bae,[5] Huiliang Wang,[2] Ping Mei,[6] Ho-Hsiu Chou,[5] Bianxiao Cui,[4] Karl Deisseroth,[3] Tse Nga Ng,[6]† Zhenan Bao[5]‡

Human skin relies on cutaneous receptors that output digital signals for tactile sensing in which the intensity of stimulation is converted to a series of voltage pulses. We present a power-efficient skin-inspired mechanoreceptor with a flexible organic transistor circuit that transduces pressure into digital frequency signals directly. The output frequency ranges between 0 and 200 hertz, with a sublinear response to increasing force stimuli that mimics slow-adapting skin mechanoreceptors. The output of the sensors was further used to stimulate optogenetically engineered mouse somatosensory neurons of mouse cortex in vitro, achieving stimulated pulses in accordance with pressure levels. This work represents a step toward the design and use of large-area organic electronic skins with neural-integrated touch feedback for replacement limbs.

Neurally controlled prosthetic devices improve mobility and independence for disabled people (*1*). The addition of tactile sensing can benefit the utility of these neuroprosthetics by enhancing motor control (*2*–*4*) and relieving phantom limb pain associated with limb loss (*5*, *6*). Thus, the implementation of human mechanoreceptor-like sensing systems would be an important step toward highly functional prosthetics.

Flexible and stretchable tactile sensors have achieved a high level of sophistication using both organic (*7*–*10*) and inorganic electronic materials (*11*–*13*). For example, Kim and co-workers recently demonstrated silicon nanoribbon strain and pressure sensor arrays that output voltage signals and stretchable multielectrode arrays for nerve stimulation (*12*). Although these technologies have focused on pushing the performance boundaries of mechanical sensitivities and large-area integration, the sensors rely on direct-current (dc) amplitude-modulated signals that may suffer from drift and noise over a long transmission distance. Furthermore, powering and obtaining readings of an enormously large density of sensors as found in human skin may not be energy-efficient using dc signal approaches. In contrast, each tactile mechanoreceptor in the human skin is a highly sophisticated, low-power biological circuit capable of transducing mechanical strain to oscillating electrical action potentials (*14*). This transduction mechanism is inherently power-efficient and robust to noise, allowing for mechanical sensations to be transmitted over long distances, such as from extremities. Previous reports on prosthetic skin systems have used a computer or microcontroller to convert the sensors' analog signals into signals that are appropriate for stimulating neurons (*4*, *12*). To enable large-scale integration, it is advantageous for the sensors to directly produce digital signals with relevant frequencies.

We present a skin-inspired artificial mechanoreceptor system (the Digital Tactile System, or DiTact) composed of flexible organic electronic materials. The organic circuits emulate the response of slow-adapting tactile receptors by encoding static pressure stimuli into digital signals whose frequency varies with stimulation intensity (Fig. 1A). Our digitizing system has three key components (Fig. 1B): (i) voltage-controlled oscillators constructed with printed organic circuits, (ii) flexible microstructured resistive pressure sensors with sensitivity in the range of human pressure-sensing capability, and (iii) a channelrhodopsin engineered specifically to enable optical neuron stimulation above 100 Hz (a range similar to that of slow-adapting mechanoreceptors).

Printed organic circuits are a promising scalable technology to use for electronic skins because of their potential for low-cost, large-area processing and compatibility with flexible substrates (*10*). Printed organic ring oscillator circuits, consisting of odd numbers of repeating inverter stages based on complementary field-effect transistors, were used (figs. S1 and S2) to generate the series of voltage spikes. Complementary ring oscillators are desirable because of their simplicity relative to other electrical oscillators, their low static power dissipation, and the dependence of the oscillation frequency on the supply voltage. By using a piezoresistive element as a component in a voltage divider, we modulated the time delay of the oscillations. As the applied force increased, the supply voltage increased and the propagation delay of the transistors was reduced, thereby increasing the frequency of the oscillations in a way that mimics the slow-adapting mechanoreceptors.

Our DiTact prototype uses a three-inverter (three-stage) ring oscillator, which is the minimum number of inverters required to maintain stable oscillations. Using fewer stages has the advantages of higher-frequency operation, lower power consumption, and smaller footprint of the devices. The complementary oscillators (fig. S1) were printed on a flexible plastic sheet (*15*) with a modified dielectric with a high dielectric constant (*16*) (see supplementary materials). The DiTact prototype relies on a change in the voltage supply to modulate the frequency output of the sensors. The oscillation frequency depends quadratically on the supply voltage (Fig. 2A) for the voltage range used in this work. A supply voltage of 11 V was chosen to set the maximum frequency to 200 Hz, so as to match the typical frequency range of biological mechanoreceptors. The supply voltage can be further reduced via reduction of the dielectric thickness, and organic oscillators operating at 3 V have been demonstrated (*17*). Because the oscillator is used in a voltage divider configuration, the impedance through the oscillator under different biasing conditions (Fig. 2B) is important for the design of the sensor circuit. To emulate human tactile perception, the DiTact system must have slow or no oscillation in the absence of pressure stimulation, and the frequency should increase with pressure (*18*). In the voltage divider configuration, the impedance of the pressure sensor must be larger than the impedance of the oscillator in the "off" state (several hundred megohms), therefore requiring gigaohm range. This is also useful for conserving power by minimizing off-state leakage. However, in the "on" state, the impedance of the sensor must be smaller than the impedance of the oscillator (10 megohms). Furthermore, the sensors should operate within the range of pressures used for typical grip control, from several to several hundred kilopascals (*19*).

To create such a wide-impedance piezoresistor, we constructed sensors composed of a carbon nanotube (CNT) composite dispersed in a polyurethane elastomer that was molded into pyramidal microstructures (Fig. 2D) (see supplementary materials). The choice of microstructures is essential to achieve the desired working range and sensing characteristics. Incorporation of pyramidal structures reduces the effective modulus (*20*) and concentrates the electric field, resulting in

[1]Department of Electrical Engineering, Stanford University, Stanford, CA, USA. [2]Department of Materials Science and Engineering, Stanford University, Stanford, CA, USA. [3]Department of Bioengineering, Stanford University, Stanford, CA, USA. [4]Department of Chemistry, Stanford University, Stanford, CA, USA. [5]Department of Chemical Engineering, Stanford University, Stanford, CA, USA. [6]Xerox Palo Alto Research Center, Palo Alto, CA, USA.
*These authors contributed equally to this work. †Present address: Department of Electrical Engineering, University of California, San Diego, CA, USA. ‡Corresponding author. E-mail: zbao@stanford.edu

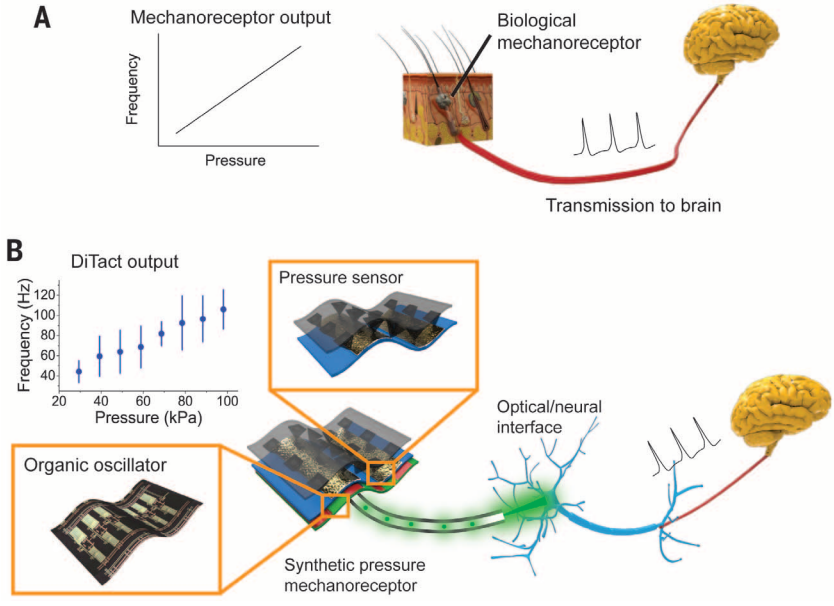

Fig. 1. DiTact concept design. (**A**) Schematic of the function of a biological somatosensory system. Voltage pulses are generated in the skin and transported to the brain. (**B**) DiTact is composed of a pressure-sensitive tactile element and an organic ring oscillator. Optogenetic pulses were used to stimulate live neurons.

improved piezoresistive properties relative to an unstructured film. Moreover, the size and spacing of the pyramidal microstructures have important effects on the sensitivity and working range (figs. S3 and S4). Because their function is based on tunneling between CNTs and an electrode, the devices show substantial voltage dependence in the sensing characteristics (Fig. 2F and fig. S5). The pressure- and voltage-dependent impedance was fitted to a mathematical model (fig. S6) for use in circuit characterization (fig. S7). When the sensor and oscillator were in series in a voltage divider, the frequency of the oscillator increased with pressure (Fig. 2G). In the on state (at 100 kPa, with all voltage dropping across the oscillator), the power dissipation of the DiTact prototype was 18.4 μW at 11 V and 2.0 μW at 6 V, which compares favorably to analog approaches. A model hand depicts how sensors could be incorporated into a prosthetic device (Fig. 2H). The electrical components were connected with stretchable silver nanowire conductors. In addition, the DiTact sensors were incorporated with a wearable glove to show the frequency variation of the voltage signal with the application of pressure in a wearable system (movie S1).

We used the pressure-induced, frequency-encoded digital signal output from the DiTact system to directly stimulate mouse cortical neurons both electrically (fig. S13) and optically (Fig. 3 and fig. S12). Although electrical stimulation is more applicable to conventional prosthetics (*4*, *12*, *21*, *22*), optogenetic stimulation is a promising new approach that we used as a reliable noncontact method to demonstrate the feasibility of interfacing with biological neural circuits. Optogenetics induces action potentials with excellent fidelity, allowing the DiTact signal to be very effectively transmitted to the target neurons. Using this approach, the output signal of the DiTact sensor was set to directly modulate the frequency of an LED light source. Light application evokes neuronal firing in neurons that express light-activated ion channels such as channelrhodopsin-2 (ChR2) or its mutations such as H134R [ChR2(HR)], which are among the standard tools for optogenetic applications.

The DiTact sensor was engineered to have a maximum frequency of 200 Hz, which is comparable to the upper limit for the generation of action potentials during tactile stimulation in humans. Consequently, the optogenetic neural interface must be capable of stimulating neurons with a frequency up to 200 Hz for several seconds. However, sustained high-frequency stimulation is difficult to achieve using conventional optogenetic channel proteins. Mutations of channelrhodopsin such as ChR2-E123A [ChETA(EA)] accelerate channel opening and closure. They are commonly used for modification of neurons for optogenetic applications and could potentially meet our requirement (*23*, *24*). However, we found that ChETA activity was not well suited in cultured pyramidal neurons to mediate spikes for extended periods of time (Fig. 3A, fig. S10, and table S1). Therefore, we engineered the channelrhodopsin hybrid C1C2 (*25*) because of its larger activity relative to ChR2 (fig. S10). The resulting construct, termed bC1C2(s/v), had larger photocurrents than ChR2(HR) and ChETA(EA), as well as fast off-kinetics (fig. S11). We expressed ChETA(EA) and bC1C2(s/v) separately in cortical fast-spiking parvalbumin-positive (PV^+) neurons and compared both constructs using whole-cell patch-amp recordings of acute slices; the results confirmed the larger photocurrents and fast kinetics of bC1C2 (s/v) (Fig. 3A, fig. S11, and table S2). bC1C2(s/v) was able to reliably evoke action potentials at frequencies up to 200 Hz for more prolonged intervals (Fig. 3, A and B), which mimics the frequency range of slow-adapting and fast-spiking tactile receptors such as Merkel cells (*26*).

To interface the digital signal from the DiTact system with live neurons, we connected the sensor output to the setup shown in Fig. 3C. The DiTact signal was conditioned via an edge detector to a 2-ms pulse that triggered the LED once per oscillation. The light pulse from the LED was used to optogenetically stimulate PV^+ neurons in an acute slice of primary somatosensory cortex from mice. For the sensor composition used in the neuron stimulation study, the frequency exhibited a sublinear dependence on the pressure

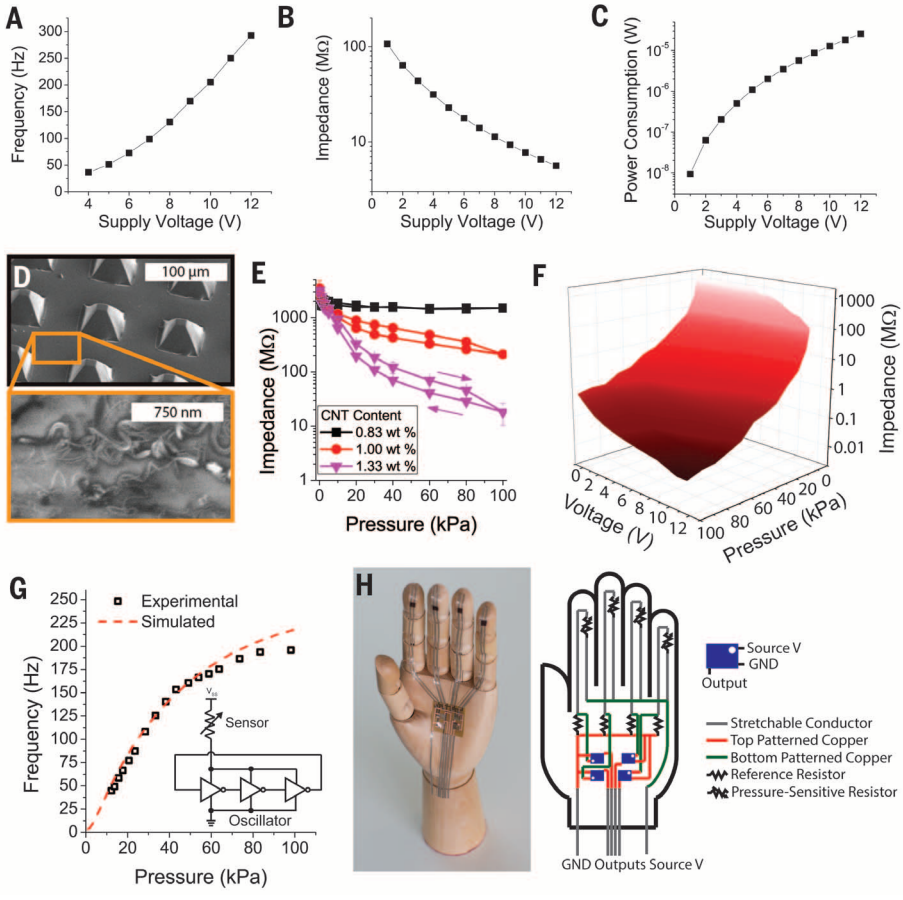

Fig. 2. Oscillator and pressure sensor characteristics and integration. (**A** to **C**) Frequency, impedance, and power dissipation as a function of supply voltage for the oscillators. (**D**) Scanning electron micrographs of the pyramids and the elastomer-CNT composite used to fabricate the piezoresistive sensors. (**E**) Pressure response of sensors as a function of CNT concentration. (**F**) Three-dimensional contour plot of impedance as a function of pressure and voltage. (**G**) Plot of frequency output as a function of pressure for an example DiTact sensor (see supplementary materials for description of circuit simulation). (**H**) Image and circuit schematic of a model hand with DiTact sensors on the fingertips connected with stretchable interconnects.

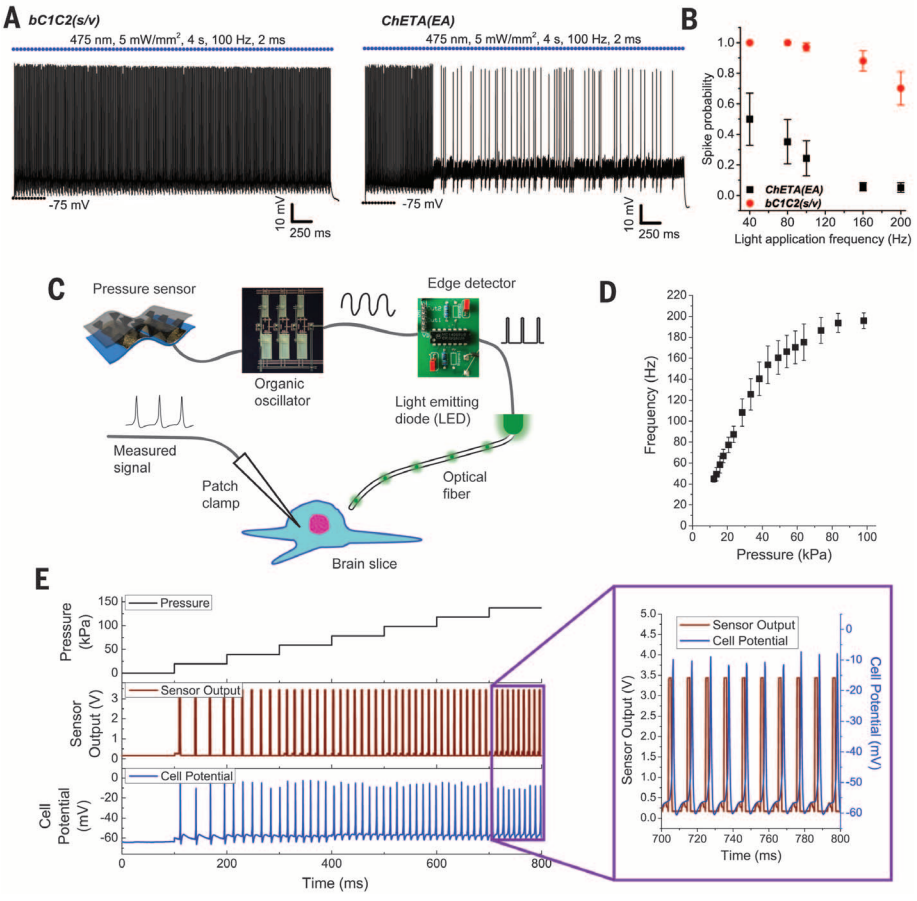

Fig. 3. Optogenetic stimulation of somatosensory cortex neurons using DiTact. (**A**) Time-resolved voltage traces of cortical fast-spiking PV^+ interneurons expressing bC1C2(s/v) (left) and ChETA (EA) (right). Cells were recorded using whole-cell patch clamping in acute slice of mice medial prefrontal cortex. Neurons were stimulated for 4 s with pulsed 475-nm light (5 mW/mm^2, pulse width 2 ms) at 100 Hz with to evoke action potentials. Spike probability is at 100% in bC1C2(s/v)-expressing neuron and decreases in ChETA(EA)-expressing neuron during prolonged stimulation. (**B**) Summary of spike probability in response to light stimulation applied at frequencies from 40 to 200 Hz. ChETA(EA), n = 16; bC1C2(s/v), n = 10. All error bars denote SEM; n indicates number of cells. (**C**) Setup of the optoelectronic stimulation system for pressure-dependent neuron stimulation. (**D**) Frequency output recorded from in vitro somatosensory cortical mouse neurons as a function of the pressure applied to the DiTact sensor. The error bars represent one standard deviation from 10 samples. Individual trials are shown in fig. S13D. (**E**) Correlation among pressure, sensor output, and cell potential. The expanded section shows that the neurons' action potentials closely follow the pulses from the LED.

(Fig. 3D). The neurons fired in accordance with the stimulation pulse, which was generated at frequencies determined by the pressure applied to the DiTact system (Fig. 3E). The output of the DiTact system had pressure-dependent frequency characteristics with a threshold and range similar to those of biological mechanoreceptors (fig. S12).

Our system currently encodes static pressure stimuli. To fully mimic the properties of biological mechanoreceptors, it will be important to implement temporal adaptation to both static and nonstatic stimuli (*18*)—for example, an increased firing rate due to moving stimuli (e.g., nonstatic brushing action) and decreased firing rates due to constant stimuli (static contact force). To demonstrate the compatibility of the DiTact approach with electrical stimulation methods, we coupled an inorganic oscillator to the pressure sensor, and the resulting frequency signal was successfully used to stimulate hippocampal neurons in a multielectrode array (fig. S13). The compatibility of the DiTact sensor with optogenetic stimulation of somatosensory cortex interneurons (Fig. 3) and parvalbumin neurons (fig. S12B), as well as electrical stimulation of hippocampal neurons (fig. S13), suggests that the system would be compatible with other fast-spiking neurons, including peripheral nerves.

Our DiTact sensors encode pressure stimulation magnitude with sublinear digital responses similar to human mechanoreceptors. The output of the sensors can stimulate in vitro neurons both electrically and optically with engineered optogenetic neurons that respond to the range of human action potential frequencies. This system can be potentially integrated over large areas as electronic skins for conventional neural prosthetics or optogenetic-based prosthetic interfaces. Furthermore, the digital nature of the output could be advantageous in high-density prosthetic sensor systems, using strategies similar to code division multiple access (CDMA) that allow for greater bandwidths with fewer interconnections.

REFERENCES AND NOTES

1. L. R. Hochberg *et al.*, *Nature* **485**, 372–375 (2012).
2. J. E. O'Doherty *et al.*, *Nature* **479**, 228–231 (2011).
3. A. Abbott, *Nature* **442**, 125–127 (2006).
4. S. Raspopovic *et al.*, *Sci. Transl. Med.* **6**, 222ra19 (2014).
5. M. Lotze *et al.*, *Nat. Neurosci.* **2**, 501–502 (1999).
6. D. W. Tan *et al.*, *Sci. Transl. Med.* **6**, 257ra138 (2014).
7. S. C. B. Mannsfeld *et al.*, *Nat. Mater.* **9**, 859–864 (2010).
8. G. Schwartz *et al.*, *Nat. Commun.* **4**, 1859 (2013).
9. M. Kaltenbrunner *et al.*, *Nature* **499**, 458–463 (2013).
10. T. Sekitani *et al.*, *Science* **326**, 1516–1519 (2009).
11. D.-H. Kim *et al.*, *Science* **333**, 838–843 (2011).
12. J. Kim *et al.*, *Nat. Commun.* **5**, 5747 (2014).
13. K. Takei *et al.*, *Nat. Mater.* **9**, 821–826 (2010).
14. E. P. Gardner, *Touch* (eLS/Wiley Online Library, 2001).
15. T. N. Ng *et al.*, *Sci. Rep.* **2**, 585 (2012).
16. P. Mei *et al.*, *Appl. Phys. Lett.* **105**, 123301 (2014).
17. T. Sekitani, U. Zschieschang, H. Klauk, T. Someya, *Nat. Mater.* **9**, 1015–1022 (2010).
18. M. Knibestöl, *J. Physiol.* **245**, 63–80 (1975).
19. D. A. Nowak, J. Hermsdörfer, *Mov. Disord.* **20**, 11–25 (2005).
20. B. C. K. Tee *et al.*, *Adv. Funct. Mater.* **24**, 5427–5434 (2014).
21. A. Canales *et al.*, *Nat. Biotechnol.* **33**, 277–284 (2015).
22. I. R. Minev *et al.*, *Science* **347**, 159–163 (2015).
23. L. A. Gunaydin *et al.*, *Nat. Neurosci.* **13**, 387–392 (2010).
24. J. Mattis *et al.*, *Nat. Methods* **9**, 159–172 (2012).
25. H. E. Kato *et al.*, *Nature* **482**, 369–374 (2012).
26. H. Haeberle, E. A. Lumpkin, *Chemosens. Percept.* **1**, 110–118 (2008).

ACKNOWLEDGMENTS

B.C.-K.T., A.C., A.B., and Z.B. conceived the experiments; T.N.N., P.M., B.C.-K.T., K.T., and H.W. worked on equipment and fabricated oscillators; A.C. and B.C.-K.T. designed pressure sensors and A.C. and H.-H.C. characterized them; B.C.-K.T., A.K.N., and A.C. implemented measurement electronics; A.B. and K.D. engineered the channelrhodopsin protein; A.B., A.C., A.K.N., and A.T. performed optogenetic measurements; B.C.-K.T., A.M., and Z.C.L. did measurements using electrical stimulation of neurons; W.-G.B. improved data visualization; B.C.-K.T., A.C., A.B., and Z.B. wrote the manuscript; and all authors reviewed and critiqued the results and made key revisions to the manuscript. We thank N. Liu for taking SEM images and Lubrizol Co. for supplyingSG80A elastomer for the pressure sensors. Supported by the Xerox Foundation; the MSIP (Ministry of Science, ICT and Future Planning), Korea, under the IT Consilience Creative Program (grant NIPA-2014-H0201-14-1001) supervised by the National IT Industry Promotion Agency; Agency for Science Technology and Research Singapore (A*STAR); and Samsung Electronics.

SUPPLEMENTARY MATERIALS

www.sciencemag.org/content/350/6258/313/suppl/DC1
Materials and Methods
Figs. S1 to S14
Tables S1 and S2
Movie S1
References (*27*–*33*)

16 February 2015; accepted 7 August 2015
10.1126/science.aaa9306

Science
AAAS

A skin-inspired organic digital mechanoreceptor
Benjamin C.-K. Tee *et al.*
Science **350**, 313 (2015);
DOI: 10.1126/science.aaa9306